

Decoding conformal field theories: from supervised to unsupervised learning

En-Jui Kuo,^{1,2} Alireza Seif,^{1,2,3} Rex Lundgren,^{2,4} Seth Whitsitt,^{2,4} and Mohammad Hafezi^{1,2,5}

¹Department of Physics, University of Maryland, College Park, MD 20742, USA

²Joint Quantum Institute, NIST/University of Maryland, College Park, MD 20742, USA

³Pritzker School of Molecular Engineering, University of Chicago, Chicago, IL 60637

⁴Joint Center for Quantum Information and Computer Science,
NIST/University of Maryland, College Park, MD 20742, USA

⁵Department of Electrical and Computer Engineering,
University of Maryland, College Park, Maryland 20742, USA

We use machine learning to classify rational two-dimensional conformal field theories. We first use the energy spectra of these minimal models to train a supervised learning algorithm. We find that the machine is able to correctly predict the nature and the value of critical points of several strongly correlated spin models using only their energy spectra. This is in contrast to previous works that use machine learning to classify different phases of matter, but do not reveal the nature of the critical point between phases. Given that the ground-state entanglement Hamiltonian of certain topological phases of matter are also described by conformal field theories, we use supervised learning on Rényi entropies, and find that the machine is able to identify which conformal field theory describes the entanglement Hamiltonian with only the lowest few Rényi entropies to a high degree of accuracy. Finally, using autoencoders, an unsupervised learning algorithm, we find a hidden variable that has a direct correlation with the central charge and discuss prospects for using machine learning to investigate other conformal field theories, including higher-dimensional ones. Our results highlight that machine learning can be used to find and characterize critical points and also hint at the intriguing possibility to use machine learning to learn about more complex conformal field theories.

Introduction.— Conformal field theories (CFT), which are quantum field theories with conformal invariance, appear in many areas of physics including condensed matter, statistical physics, and string theory [1, 2]. This procedure turns out to be especially powerful in two spacetime dimensions (one spatial dimensional and one temporal dimension), where the conformal group is infinite-dimensional, and certain two-dimensional CFTs may be classified by a finite number of primary fields [1, 2]. These CFTs, which are realized in a number of physically relevant systems, including the low-energy theory of the quantum critical point of the transverse-field Ising model [3], the edge states (along with the ground-state entanglement Hamiltonian) of fractional quantum Hall systems [4, 5], and the Polyakov action describing the world sheet in string theory [6], are important for being rare examples of analytically tractable strongly-interacting quantum field theories.

Therefore, given some data of a quantum system, it is important to identify whether that system is described by a CFT. This data, obtained from either experimental measurements or numerical simulations, could be the few lowest energy levels of a given Hamiltonian or Rényi entanglement entropies, which can be measured by probing multiple copies of the system's state [7–11]. In particular, it is interesting to ask if this information can be used to detect whether a system is at a critical point, and what kind of CFT describes it the best. To address this question, we turn to machine learning.

Machine learning has been increasingly used to study a wide range of problems in different areas of physics over the past few years [12]. Notable examples include: classifying phases of matter [13–15], studying non-equilibrium dynamics of physical systems [16–18], studying the string theory landscape [19] and AdS/CFT correspondence [20], simulating dynamics of quantum systems [21], quantum state tomogra-

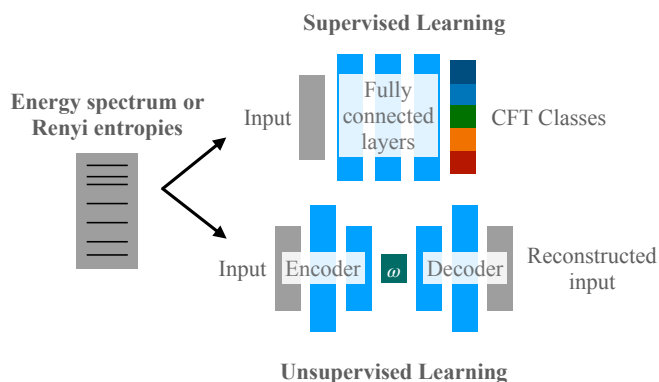


FIG. 1. Schematic illustration of the machine-learning algorithms to identify different CFTs. The pre-processed energy spectrum or Rényi entropies are stored into a vector that serves as an input to the algorithms. We consider two scenarios: supervised learning, and unsupervised learning. In the former, labels of the CFT class are provided to a neural network classifier, which predicts the CFT theory that describes the given CFT data. In the latter, we use an autoencoder neural network, which learns an efficient representation of the energy spectra. The first half of the network acts as an encoder that maps the input to a single scalar variable ω , and the second half decodes ω and reconstructs the original input. We find that ω is directly correlated to the central charge.

phy [22, 23], and augmenting capabilities of quantum devices [24, 25].

In this work, we use both unsupervised and supervised machine learning to investigate various two-dimensional CFTs, as sketched in Fig. 1. For supervised learning, we use a deep neural network. Our first training data set is the lowest energy levels of exactly-solvable two-dimensional CFTs. The chosen

CFT models include the well-known Ising critical point and $SU(2)_k$ anyonic chain parafermionic model (see Table I for a full list). We then ask the machine to locate and predict the nature of critical points of quantum spin-chains to high accuracy. By looking at the confidence of the network, we are able to correctly identify the value of the critical point. Remarkably, our approach requires a single system size, whereas common methods (such as entanglement scaling [26]) require finite-size scaling. Given that the entanglement spectra (ES) of various topological phases of matter are also described by CFTs [5, 27], we train our network with the lowest few Rényi entropies. While the relationship between Rényi entropies and ES is non-linear and requires all Rényi entropies to solve for the ES exactly, we are able to extract the CFT that describes the ES of two different spin-ladder systems to high accuracy with only having access to the lowest few Rényi entropies. Finally, we use the autoencoder algorithm [28], i.e. an unsupervised learning algorithm, and we find that the value of the hidden variable is directly related to the central charge. This gives us a hint that the machine can detect the complexity of CFTs.

Machine learning and CFT basics.—We first review the CFT knowledge needed to generate our training data (see Ref. [1] for a detailed review of CFTs and Ref. [28] for machine learning), which is taken to be the lowest twenty energy levels of a finite-size model. We take our system to have periodic boundary conditions, although our approach can be readily generalized to include other boundary conditions. In this work, we restrict ourselves to rational CFTs (RCFTs), which only contain a finite number of primary fields, and we furthermore focus on CFTs with field content such that they are modular invariant (see the Supplementary Material A for definitions and details). Our methods may easily be applied to CFTs with non-modular invariant field content.

The discrete energy levels (in units of $2\pi/L$, where L is the length of the system, and $\hbar = 1$) of a generic finite one-dimensional model which flows to a CFT is given by [1]

$$E = E_1 L + E_0 + \frac{2\pi v}{L} \left(-\frac{c}{12} + h_L + h_R \right), \quad (1)$$

where E_1 , E_0 , and v are non-universal constants, and c is the central charge of the CFT. We are also omitting subleading dependence on L due to corrections to the scaling limit. Here, $h_L = h_L^{(0)} + m_L$ and $h_R = h_R^{(0)} + m_R$, where $h_L^{(0)}, h_R^{(0)}$ correspond to scaling dimension of the primary fields and m_L and m_R are non-negative integers describing the descendant fields.

As a definite example, we now discuss the structure of the primary descendant fields for the critical Ising model, the simplest non-trivial CFT and an example of a Virasoro minimal model. With modular invariance imposed, there are three primary fields for this model, $h_{L,R}^{(0)} = 0, \frac{1}{16}$ and $\frac{1}{2}$. The number of descendant fields can be calculated by expanding the so-called character function, as reviewed in the Supplementary Material. Upon doing so, one finds the lowest ten energy levels of this CFT (with the ground state energy set to zero)

Model	Class	Central charge
(A_3, A_2) - Ising	0 ●	1/2
(A_4, A_3) - Tricritical	1 ●	7/10
(D_4, A_4)	2 ●	4/5
(A_6, D_4)	3 ●	6/7
\mathbb{Z}_4 parafermion	4 ●	1
\mathbb{Z}_5 parafermion	5 ●	8/7
\mathbb{Z}_6 parafermion	6 ●	5/4
$N = 1$ SCFT, $k = 5$	7 ●	81/70
$N = 1$ SCFT, $k = 7$	8 ●	55/42
$(A_{k+1}, A_k), k = 5 - 8$	9 - 12	$1 - 6/(k(k+1))$

TABLE I. List of all conformal field theories, i.e. classes, we include in our supervised training. We use color dots to indicate the CFT shown in Figs. 2 and 3.

are $\frac{2\pi v}{L} \times \{0, \frac{1}{8}, 1, \frac{9}{8}, \frac{9}{8}, 2, 2, 2, 2, \frac{17}{8}\}$. The energy spectrum of some of the other models we consider are discussed in the Supplemental Material, and the list of all CFTs we consider for unsupervised learning is given in Table I. We stress that this is by no means a complete list of RCFTs, as there are actually an infinite number of them.

We use a neural network to classify the input CFT spectra into their corresponding CFT classes (see Fig. 1). Specifically, we use the following neural network architecture with the input and output being the first 15 energy levels and their corresponding CFT class labels from the 13 CFT classes in Table I: $\mathbb{R}^{15} \xrightarrow{\text{linear}} \mathbb{R}^5 \xrightarrow{\text{relu}} \mathbb{R}^{13} \xrightarrow{\text{softmax}} \mathbb{R}^{13}$. The layers are represented by their domain and the expressions above the arrows indicate the activation functions of each layer. To train the network we take samples of the energy spectra of different CFT classes and add a noise term drawn randomly from the uniform distribution in $(-\epsilon, \epsilon)$. This is physically motivated by the existence of experimental measurement errors or subleading corrections to Eq. (1). It also serves as a form of data augmentation that can prevent overfitting [28]. We also preprocess the input such that the ground state energy is set to zero and the other energies are rescaled so that largest energy level is 1. This removes the contributions of the non-universal constants in the input data (see Supp. Mat.). We then optimize the categorical cross entropy over 3000 samples for each class with $\epsilon = 0.1$. The optimization is performed using the Adam optimizer with hyperparameters given in Ref. [29] in 2000 epochs with the batch size set to 128.

Critical spin-chains.— We now use the network trained on ideal CFT energy spectra with added noise, to make predictions for two physical models. Specifically, we feed the machine energy spectra from two many-body quantum spin models obtained using exact diagonalization. By analyzing the output of the machine, we are able to predict the location of the critical point and the type of CFT that describes it.

We first consider the transverse-field Ising model, $H_I(h) = -\sum_{i=1}^L \sigma_i^z \sigma_{i+1}^z - h \sum_{i=1}^L \sigma_i^x$. Here, σ_α^i are the Pauli matrices on site i and h is a global magnetic field. For $h = 1$, the low-energy theory of H_I is a CFT whose central charge is $c = 1/2$ (minimal model (A_3, A_2)). We perform exact diagonalization

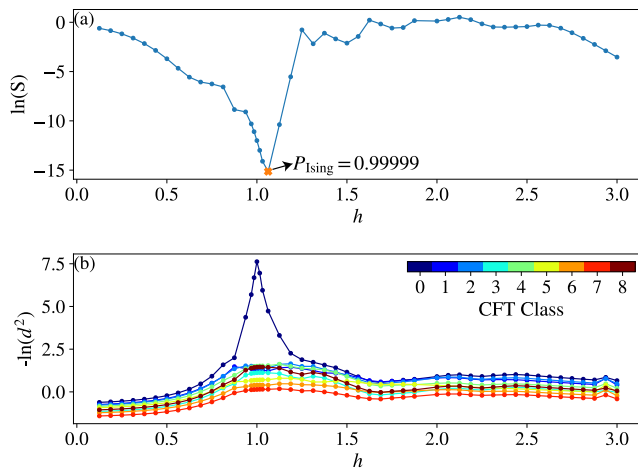


FIG. 2. Predictions of our supervised machine learning approaches on the spectrum data transverse field Ising model as a function of the transverse field h . (a) The confidence, i.e entropy, S , of the neural network. (b) The Gaussian distance, d_2 , between the energy spectrum of H_{ISING} and the energy spectrum of the first 9 CFTs in Table I. The numbers in the legend refer to the CFT class.

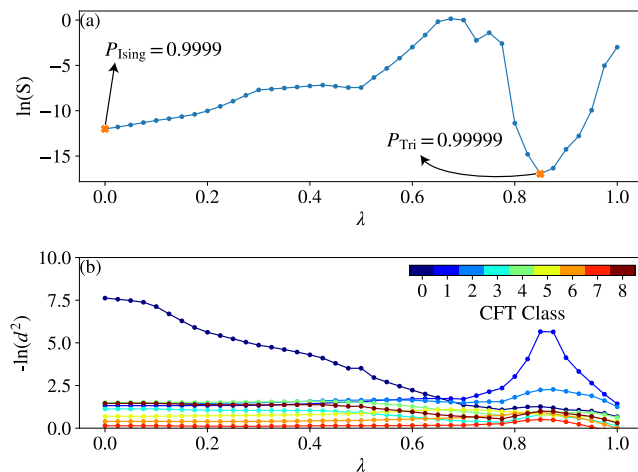


FIG. 3. Predictions of our supervised machine learning approaches on a spin model composed of the transverse field Ising Hamiltonian with $h = 1$ (see Fig. 2) with added three-body interaction terms that are controlled by a parameter λ . (a) The entropy of probabilities, S , of the neural network. (b) The Gaussian distance, d_2 , between the energy spectrum of H_T and the energy spectrum of the first 9 CFTs in Table I. The numbers in the legend refer to the CFT class.

(for $L = 22$) for different h and feed the energy spectrum into the network. In Fig. 2a, we observe that the entropy S of the output layer, $S = -\sum_i p_i \ln p_i$, where p_i corresponds to the i th value of the output softmax layer, is minimal at $h = 1$ and has a large probability of being described by minimal model (A_3, A_2) . This indicates that the network has not only correctly predicted the location of the critical point for this model, but also the nature of the critical point.

Before moving on to the next model, we discuss another

quantitative approach to identifying CFTs from energy spectra. We consider a clustering algorithm, using the Gaussian kernel of the euclidean distance, i.e., $d_2(x, c_m) = e^{-\|x - c_m\|_2^2}$, where x is the input spectra and c_m is the center of the m 'th cluster [28]. In our work, the ideal center of clusters is known from the CFT theory. Therefore, given an energy spectra, we calculate and compare the kernel on the rescaled input and the cluster centers of each CFT. In Fig. 2b, we plot d_2 for the Ising model and various CFTs. We observe that d_2 is peaked around the critical point for only the Ising model (Fig 2b), similar to the neural network approach (Fig 2a). However, we believe the neural network approach will be more reliable as it does not rely on a single energy spectrum.

We now move to a more complicated model, which has two critical points described by different CFTs and both two-body and three-body interactions. The Hamiltonian of this model, originally introduced in Ref. [30], is given by $H_T = 2H_1(1) + \lambda H_3$, where $H_3 = \sum_j \sigma_j^x \sigma_{j+1}^z \sigma_{j+2}^z + \sigma_j^z \sigma_{j+1}^x \sigma_{j+2}^x$. For $\lambda = 0$, this model is described by minimal model (A_3, A_2) as discussed above. When $\lambda \approx 0.856$, the low-energy theory of this model is described by a different minimal model, (A_4, A_3) . Again, we feed the network the many-body energy spectrum for various λ . In Fig. 3a we observe that the machine is correctly able to identify the location and underlying CFTs of the two critical points with high accuracy. Similar results are seen for the Gaussian kernel method (Fig. 3b).

Rényi Entropies.— We now consider training with Rényi entropies. This is motivated by the fact that the (bipartite real-space) entanglement Hamiltonian, H_e , of two-dimensional topological phases is often described by (either chiral or non-chiral) one-dimensional CFTs [5, 27]. Unfortunately, it is hard to experimentally measure the eigenvalues of H_e , i.e. the ES (although there are various theoretical proposals on how to do so [31]). Instead, one typically measures the Rényi entropy by preparing multiple copies of the state and interfering them [9]. Furthermore, one can calculate S_n with quantum Monte Carlo, making the calculation of entanglement more manageable for larger systems [11, 32]. We will demonstrate that, given a critical H_e [33], one can train neural-networks with Rényi entropies to correctly identify the underlying CFT.

The n -th Rényi entropy is defined as $S_n = \frac{1}{1-n} \ln \text{Tr} \rho_A^n$, where ρ_A is the reduced density matrix and n is some positive integer not equal to one. The ES (eigenvalues of $-\ln(\rho_A)$) can be obtained with knowledge of S_n for all n . In practice one can obtain an estimate of ES with only a finite number of S_n [7, 32]. In these approaches, the ES is obtained from the roots of a polynomial equation, whose coefficients are related to Rényi entropies through Newton's identities. However, root-finding algorithms are sensitive to errors in the coefficients, making such schemes unstable in the presence of errors in S_n measurements [34]. We approach this problem using machine-learning.

If H_e is a CFT, the i th ES level is given by $\epsilon_i = \epsilon_0 + \epsilon_1 L + \frac{2\pi v}{L} n_i$, where n_i is the universal part of the spectrum (see Eq. (1)). We remind the reader n_i is different set of num-

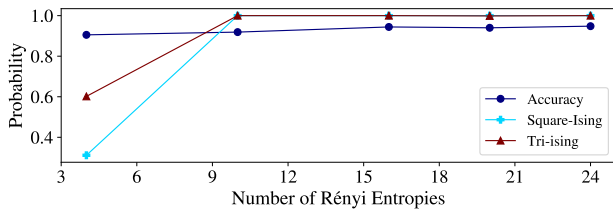


FIG. 4. Probability of the neural network predicting the correct CFT of the entanglement Hamiltonian for the square (triangle) Ising model, depicted with square (diamond), as a function of number of Rényi entropies included in training samples. The overall accuracy of the network is benchmarked using the test data, shown as dark blue circles.

bers for each respective CFT. S_n , which is only a function of $\frac{v}{L}$ (for a given CFT), can then be written as

$$S_n = (1 - n)^{-1} \ln \left[\frac{\sum_{i=0} e^{-n \frac{2\pi v}{L} n_i}}{\sum_{i=0} e^{-\frac{2\pi v}{L} n_i}} \right]. \quad (2)$$

We restrict the sum in Eq. (2) to the lowest 100 ES levels. For training, we consider a finite range of $\frac{v}{L} \in (0.2, 10)$. This range is chosen not to include large (small) $\frac{v}{L}$ where excited state information is washed out (choice of cut-off plays an important role). Also, note that for larger n , S_n becomes less dependent on the cut-off by definition. Thus, in the chosen range of $\frac{v}{L}$, the choice of cut-off, i.e. simply truncating the sum, has little effect on our results.

Instead of each sample being a vector of energy levels as in the previous section, it is a vector of Rényi entropies, (S_2, S_3, \dots) . Here, we include up to 28 Rényi entropies, starting with S_2 . We train our machine with 10000 different samples for each CFT class (same classes used for energy spectrum training). We generate the data uniformly by randomly choosing $\frac{v}{L}$. We obtain a training accuracy of up to 94 % depending on the number of S_α included. Generally, upon increasing the number of S_α included, the accuracy increases (see Fig. 4). We now describe the training process. The network architecture is: $\mathbb{R}^n \xrightarrow{\text{relu}} \mathbb{R}^{100} \xrightarrow{\text{relu}} \mathbb{R}^{20} \xrightarrow{\text{relu}} \mathbb{R}^{15} \xrightarrow{\text{relu}} \mathbb{R}^{13} \xrightarrow{\text{softmax}} \mathbb{R}^{13}$ where n is the number of Rényi entropies we use. Similar to the classification of the energy spectra, we train the network by optimizing the cross-entropy using the Adam optimizer [29], this time with 500 epochs and batch size set to 128.

We now test our model on two exactly-solvable systems [27]. The (unnormalized) ground state of these two models, which can be regarded as quantum spin ladders, can be written as $|\psi(z)\rangle = \sum_{\tau, \sigma} [T(z)]_{\tau, \sigma} |\tau\rangle |\sigma\rangle$. For the square ladder model,

$$[T(z)]_{\tau, \sigma} = \prod_{i=1}^L z^{(\sigma_i + \tau_i)/2} f(\sigma, \tau), \quad (3)$$

and for the triangle ladder model,

$$[T(z)]_{\tau, \sigma} = \prod_{i=1}^L z^{(\sigma_i + \tau_i)/2} f(\sigma, \tau) (1 - \sigma_i \tau_{i+1}). \quad (4)$$

Here, σ_i and τ_i are either 0 or 1 and $f(\sigma, \tau) = (1 - \sigma_i \tau_i)(1 - \sigma_i \sigma_{i+1})(1 - \tau_i \tau_{i+1})$. We then trace out one of the legs of the ladder. The spectrum of ρ_A is identical to the spectrum of the following matrix, $M = \frac{1}{\Xi(z)} [T(z)]^T T(z)$, where $\Xi(z)$ ensures ρ_A is properly normalized. One can interpret $T(z)$ as the transfer matrix of certain two-dimensional classical models with known critical points. Hence, if $T(z)$ is critical, H_e will be critical [27]. The critical point of the square (triangle) ladder is $z_c \approx 3.8(11.1)$. The critical theories of the square and the triangle ladder models are described by minimal models (A_3, A_2) and (D_4, A_4) respectively. We numerically calculate S_n (from M) at z_c for $L = 18$ and use these numerical results as input into our trained neural-network. We remarkably find that the neural-network correctly predicts the CFT that describes H_e for both models with high accuracy. As expected, this accuracy generally increases as one increases the number of S_α included in the training set (see Fig. 4).

Unsupervised Learning.— We now turn to using unsupervised learning to explore two-dimensional CFTs. Our data consists of three families of CFTs (see Fig. 5 for the list of CFTs used for unsupervised training). We use autoencoders [35] to find a compressed representation of the CFTs (see Fig. 1). Previously, autoencoders have been able to detect the order parameter, i.e. magnetization, in the Ising model [14]. The autoencoder is comprised of an encoder function $\omega = f(\mathbf{x})$ and a decoder function $\mathbf{r} = g(\omega)$, where the hidden variable ω encodes a compressed representation of the input \mathbf{x} . The hidden variable is used by the decoder to find the reconstruction \mathbf{r} . By restricting the dimension of ω , the network only approximately reconstructs the input, however, it learns the important features of the training data and encodes it in ω . Each class has 100 examples which consists of the lowest 100 energies of the CFT (with same noise added as our energy based classification section.)

We train different autoencoders on a set of energies corresponding to different CFT classes by minimizing $C = \frac{1}{N_m} \sum_m \|\mathbf{r}_m - \mathbf{x}_m\|_2^2$, where the sum is taken over N_m examples in the training set. The x_m is a input of the first layer and r_m is a output of the last layer. \mathbf{x} contains the first 100 energy levels. We use the following architecture for the autoencoder:

$$\mathbb{R}^{100} \xrightarrow{\text{relu}} \mathbb{R}^5 \xrightarrow{\text{sigmoid}} \mathbb{R}^h \xrightarrow{\text{relu}} \mathbb{R}^5 \xrightarrow{\text{sigmoid}} \mathbb{R}^{100}, \quad \text{where}$$

h is the dimension of the hidden variable ω . We train the network by optimizing C , using the Adam optimizer with 2000 epochs and batch sizes equals to 256. We consider the simplest case of $h = 1$ and show the value of ω for different CFT spectra in Fig. 5. We observe that within a single family of CFTs, the magnitude of the hidden variable has positive correlation with k , and hence the central charge.

Finally, we note recent work used supervised machine learning to investigate CFT correlation functions and the

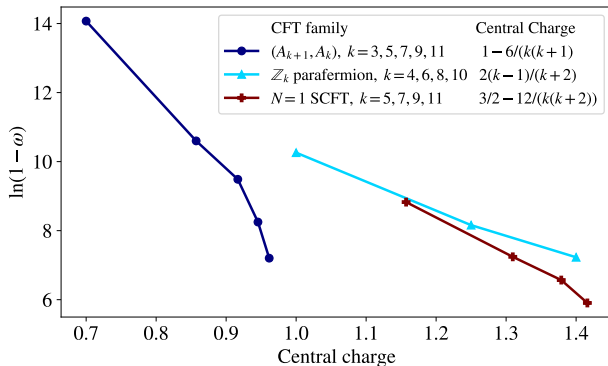


FIG. 5. Unsupervised learning: The hidden variable as a function of the central charge for different CFT families (different colors and markers). We observe that within a family, the one-dimensional hidden variable ω is a monotonous function of the central charge.

emergence of conformal invariance [36]. Recently, it is been demonstrated that for the specific conformal field theory like Ising CFT, one can use an unsupervised learning method to classify them without dimensional reduction [37, 38]. However, the information of the critical point should be known in advance which is different from our work. Our work specifies conformal field theory by using the hidden variable when restricting to a single-family without knowing the critical point in advance. In the future, it would be interesting to include correlation functions in our unsupervised training to see if could distinguish different families of CFTs.

Discussion.— We have investigated possible applications of machine learning for CFTs. By supervised training with two-dimensional CFT energy spectra and Rényi entropy, we find our network can identify the critical points of many-body models to high-accuracy. In the case of energy spectra, our network is also able predict the location of critical points. For the unsupervised learning part, we see that the latent variable increases with the central charge of the CFT (for a given CFT family) suggesting that machine learning can detect the complexity of CFTs.

There are several directions where our work can be readily extended. For example, the entanglement Hamiltonian of a CFT can always be written in terms of the boost operator [39, 40], to which our methods may be applied. For critical one-dimensional systems, the entanglement spectra for particular entanglement cuts correspond with the spectra of boundary CFTs [41–43], which are also known [44–46]. We believe the methods developed in this Letter can be straight forwardly extended to these CFTs. Including more complicated two-dimensional CFTs in the energy spectrum training process (such as non-unitary CFTs [47–50], floquet CFTs [51–53], CFTs with continuous scaling dimensions [41], and the product of two CFTs [54]) would also be a worthwhile avenue to pursue.

Finally, it would be extremely interesting to use machine-learning techniques investigate higher-dimensional CFTs

where the conformal group is no longer infinite dimensional and much less is understood about the structure of the energy spectrum. The most convenient geometry for exact diagonalization in 2+1D is the torus, where the low-energy energy spectrum is a universal fingerprint of the universality class described by the CFT. Recent studies have obtained the low-energy torus spectra for CFTs in several universality classes, including the Wilson-Fisher CFTs and related \mathbb{Z}_2 confinement transitions [55–57], the fermionic chiral (or Gross-Neveu) fixed points [58], and QED3 [59]. In principle, the data obtained in these studies could be used as training data for a generalization of the present work to 2+1D, including the unsupervised learning portion. One could then imagine training with both standard order parameters [13–15] and energy spectra to establish phase diagrams and the nature of critical points in higher-dimensions.

We are grateful to M. Dalmonte, W. DeGottardi, and M. A. Rajabpour for useful discussions and S. Tanaka for sharing numerical data. E.J.K., A.S. and M.H. acknowledge support from AFOSR-MURI FA95501610323, U.S. Department of Energy, Quantum Systems Accelerator program and the Simons Foundation. A.S. is additionally supported by a Chicago Prize Postdoctoral Fellowship in Theoretical Quantum Science. R.L. acknowledges support by the DoE BES QIS program (award No. DE-SC0019449), AFOSR, DoE ASCR Quantum Testbed Pathfinder program (award No. DE-SC0019040), NSF PFCQC program, NSF PFC at JQI, ARO MURI, and ARL CDQI. S.W. acknowledges support from the NIST NRC Postdoctoral Associateship award.

Appendix A: Two-dimensional conformal field theories

In this section, we summarize the important aspects of the two-dimensional CFTs relevant to the results presented in this paper. Detailed discussions of two-dimensional CFTs can be found in Refs. [1, 2, 60].

The Virasoro minimal models are the complete set of unitary CFTs with a finite number of irreducible representations under the Virasoro algebra; however, if a CFT is also invariant under a larger symmetry group, it may be an RCFT by having a finite number of irreducible representations under the extended symmetry algebra. This is the case for parafermionic models and superconformal minimal models, which contain conserved parafermionic and fermionic currents respectively.

The two-dimensional CFTs we consider may be specified by a central charge, c , and a finite set of holomorphic and anti-holomorphic fields, denoted by $\phi_{h_L}(z)$ and $\phi_{h_R}(\bar{z})$ respectively. Here, we use complex coordinates $z = x + it$ and $\bar{z} = x - it$ to parametrize the two-dimensional coordinates (x, t) . The numbers (h_L, h_R) , which are called the conformal dimensions of the associated primary fields, are real numbers which are generically independent. With this data, it is known that the finite-size energy spectrum of a two-dimensional CFT (in units of $2\pi/L$) is given by Eq. (1), where the lowest states correspond to primary fields, and the higher states are known

as descendants. However, the degeneracy of the states corresponding to primary operators and their descendants can be nontrivial [61].

We now review the degeneracy structure of the energy spectrum. In this work, we simply present the result for the partition function and refer the reader to Ref. [1] for details. We consider an RCFT on a torus with complex-valued periods equal to ω_1, ω_2 , and define the modular parameter of the torus as $\tau = \omega_2/\omega_1$. Then we can write the partition function of an RCFT on the torus as [1]

$$Z(\tau) = \sum_{h_L, h_R} M_{h_L, h_R} \chi_{h_L}(\tau) \chi_{h_R}(\bar{\tau}), \quad (\text{A1})$$

where

$$\chi_{h_L, R}(\tau) = \sum_{n=0}^{\infty} \dim(h_{L, R} + n) q^{h_{L, R} + n - c/24} \quad (\text{A2})$$

are the so-called characters associated with a given primary operator $\phi_{h_L, R}$. Here, M_{h_L, h_R} counts the number of occurrences of the primary $\phi_{h_L}(z) \times \phi_{h_R}(\bar{z})$ in the CFT, and we use the parametrization $q = e^{2\pi i \tau}$.

The reason for considering the partition function on the torus is to demand that $Z(\tau)$ be left invariant under the modular transformations $\tau \rightarrow \tau + 1$ and $\tau \rightarrow -1/\tau$. This strongly constrains the structure of the spectrum investigated in the main body of the paper. It is believed that only modular invariant CFTs can be realized by a one-dimensional quantum lattice model, although non-modular invariant CFTs may arise as boundaries of two-dimensional lattice theories with bulk topological order [62]. In the following we discuss the form of χ_{h_L} for the CFT families we are interested in.

1. Virasoro minimal models

In Virasoro minimal models, the central charge of the Virasoro algebra takes values of the type [63],

$$c_{p, q} = 1 - 6 \frac{(p - q)^2}{pq}, \quad (\text{A3})$$

where p, q are coprime integers such that $p, q \geq 2$. Then the allowed conformal dimensions of the (anti)holomorphic representations are

$$h_{r, s} = \frac{(pr - qs)^2 - (p - q)^2}{4pq}, \quad \text{with } r, s \in \mathbb{N}^* \quad (\text{A4})$$

where

$$1 \leq r \leq q - 1, \quad 1 \leq s \leq p - 1. \quad (\text{A5})$$

The (p, q) and (q, p) models are the same.

From the previous discussion, we know that the allowed values of (h_L, h_R) and their degeneracies can be inferred by the set of modular invariant partition functions on the torus.

The complete set of such partition functions has been entirely worked out for the unitary minimal models using the so-called ADE classification [64].

As a definite example, we consider the Ising CFT ($c = 1/2$), in which case there is only a single modular invariant choice of operators. If one expands the partition function in terms of the parameters $q = e^{2\pi i \tau}$, $\bar{q} = e^{-2\pi i \bar{\tau}}$, the full energy spectrum and its degeneracy can be read off from the coefficients and powers of the expansion. For the Ising CFT, the partition function turns out to be diagonal, meaning one only allows fields of the form $\phi_{h_L}(z) \times \phi_{h_R}(\bar{z})$ with $h_L = h_R$, and we can read off the spectrum from the degeneracy of q alone. Just giving the q -dependence, and keeping terms up to q^5 and the level-3 descendants, the expansion is

$$q^{\frac{1}{12}(1 - \frac{6}{3(4)})} Z_{\text{ising}} = 1 + \sqrt[8]{q} + q + 2q^{9/8} + 4q^2 + 3q^{17/8} + 5q^3 + O(q^{25/8}). \quad (\text{A6})$$

This expression should be read as follows: with energies measured with respect to the ground state and in units of $2\pi/L$, we have unique states with $E = 0, 1/8, 1$, a two-fold degenerate state with $E = 9/8$, a four-fold degenerate state with $E = 2$, a three-fold degenerate state with $E = 17/8$, etc. This explains how the energy level structure of the Ising model given in the main text was obtained.

2. \mathbb{Z}_k parafermion CFTs

\mathbb{Z}_k parafermion CFTs have a central charge given by $c = \frac{2(k-1)}{k+2}$ [63]. The conformal dimensions of the primary fields of these CFTs are

$$h_{r, s} = \frac{r(r+2)}{4(k+2)} - \frac{s^2}{4k}, \quad (\text{A7})$$

where $r = 0, 1, \dots, k$ and $s = -r + 2, -l + 4, \dots, r$. The associated character is [65]

$$\chi_{(r, s)}(\tau) = \eta(q) c_s^r(q), \quad (\text{A8})$$

where $c_s^r(q)$ is given by

$$c_s^r(q) = \sum_{l, m=0}^{\infty} (-1)^{l+m} q^{(k+r)lm + \frac{1}{2}(l+1)l + \frac{1}{2}(m+1)m} \times \frac{q^{-\frac{c-1}{24} + h_{r, s}}}{\eta(q)^3} \left(q^{\frac{1}{2}l(r+s) + \frac{1}{2}m(r-s)} - q^{\frac{1}{2}l(2k-r-s+2) + \frac{1}{2}m(2k-r+s+2) + k-r+1} \right), \quad (\text{A9})$$

and $\eta(q)$ is the Dedekind eta function. The partition function is then given by

$$Z(\tau) = \sum_{s=0}^{2k-1} \sum_{r=0}^k |\chi_{r, s}(\tau)|^2. \quad (\text{A10})$$

One may show that the theories for $k = 1, 2, 3$ correspond to Virasoro minimal models, but for $k \geq 4$ we have new RCFTs. In this paper, we include parafermionic theories with $k = 4, 5, 6, 7$. The energy spectra of these models can be obtained by the q expansion of Eq. (A10).

3. $\mathcal{N} = 1$ superconformal minimal models

The $\mathcal{N} = 1$ superconformal minimal models have central charge $c = \frac{3}{2} - \frac{12}{k(k+2)}$, with $k \geq 2$ an integer [63]. The scaling dimension of the primary field is

$$h_{r,s} = \frac{[(k+2)r - ks]^2 - 4}{8k(k+2)} + \frac{1}{32} (1 - (-1)^{r+s}). \quad (\text{A11})$$

where $1 \leq r \leq k-1$ and $1 \leq s \leq k+1$. Fields with $r+s$ even have a conformal dimensions are given by:

$$h'_{r,s} = h_{r,s} + \frac{1}{2} + \delta_{r+s,2}. \quad (\text{A12})$$

The characters and partition function for this case are much more involved, and we refer the readers to Refs. [66, 67] for their explicit expressions.

Appendix B: Preprocess procedure

In this section, we discuss how to eliminate the non universal constants E_0, E_1, L, v . We refer to this procedure as preprocessing. We have the following relation,

$$E = E_1 L + E_0 + \frac{2\pi v}{L} \left(-\frac{c}{12} + h_L + h_R \right). \quad (\text{B1})$$

Let H_i be the i -th value of $h_L + h_R$, which is an integer. Notice that the lowest level, H_0 , is zero for all CFTs investigated in this work. Defining $\{X_0, X_1, \dots, X_n\}$ as our non universal energies, we have

$$X_i = E_1 L + E_0 + \frac{2\pi v}{L} \left(-\frac{c}{12} + H_i \right). \quad (\text{B2})$$

We then have the energy differences from the ground state,

$$\frac{2\pi v}{L} H_i = X_i - (E_1 L + E_0) + \frac{2\pi v}{L} \frac{c}{12}. \quad (\text{B3})$$

We then rescale the highest shifted energy to be 1. This gives a set of n preprocessed energies, $\{x_0, x_1, \dots, x_n\}$, given by

$$x_i = \frac{X_i - (E_1 L + E_0) + \frac{2\pi v}{L} \frac{c}{12}}{\frac{2\pi v}{L} H_n} = \frac{H_i}{H_n}. \quad (\text{B4})$$

We see that x_i is independent of E_0, E_1, L, v .

-
- [1] Philippe Francesco, Pierre Mathieu, and David Sénéchal, *Conformal field theory* (Springer Science, 2012).
 [2] Paul Ginsparg, “Applied conformal field theory,” arXiv preprint hep-th/9108028 (1988).
 [3] Sheer El-Showk, Miguel F. Paulos, David Poland, Slava Rychkov, David Simmons-Duffin, and Alessandro Vichi, “Solving the 3d ising model with the conformal bootstrap,” *Phys. Rev. D* **86**, 025022 (2012).

- [4] Gregory Moore and Nicholas Read, “Nonabelions in the fractional quantum hall effect,” *Nuclear Physics B* **360**, 362–396 (1991).
 [5] Hui Li and F. D. M. Haldane, “Entanglement spectrum as a generalization of entanglement entropy: Identification of topological order in non-abelian fractional quantum hall effect states,” *Phys. Rev. Lett.* **101**, 010504 (2008).
 [6] Joseph Polchinski, *String theory: Volume 1, an introduction to the bosonic string* (Cambridge university press, 1998).
 [7] H. Francis Song, Stephan Rachel, Christian Flindt, Israel Klich, Nicolas Laflorencie, and Karyn Le Hur, “Bipartite fluctuations as a probe of many-body entanglement,” *Phys. Rev. B* **85**, 035409 (2012).
 [8] AJ Daley, H Pichler, J Schachenmayer, and P Zoller, “Measuring entanglement growth in quench dynamics of bosons in an optical lattice,” *Physical review letters* **109**, 020505 (2012).
 [9] Rajibul Islam, Ruichao Ma, Philipp M Preiss, M Eric Tai, Alexander Lukin, Matthew Rispoli, and Markus Greiner, “Measuring entanglement entropy in a quantum many-body system,” *Nature* **528**, 77–83 (2015).
 [10] Hannes Pichler, Guanyu Zhu, Alireza Seif, Peter Zoller, and Mohammad Hafezi, “Measurement protocol for the entanglement spectrum of cold atoms,” *Physical Review X* **6**, 041033 (2016).
 [11] Zhaoyou Wang and Emily J Davis, “Calculating rényi entropies with neural autoregressive quantum states,” *Physical Review A* **102**, 062413 (2020).
 [12] Giuseppe Carleo, Ignacio Cirac, Kyle Cranmer, Laurent Daudet, Maria Schuld, Naftali Tishby, Leslie Vogt-Maranto, and Lenka Zdeborová, “Machine learning and the physical sciences,” arXiv preprint arXiv:1903.10563 (2019).
 [13] Juan Carrasquilla and Roger G Melko, “Machine learning phases of matter,” *Nature Physics* **13**, 431 (2017).
 [14] Sebastian J Wetzal, “Unsupervised learning of phase transitions: From principal component analysis to variational autoencoders,” *Physical Review E* **96**, 022140 (2017).
 [15] Evert PL Van Nieuwenburg, Ye-Hua Liu, and Sebastian D Huber, “Learning phase transitions by confusion,” *Nature Physics* **13**, 435 (2017).
 [16] Evert van Nieuwenburg, Eyal Bairey, and Gil Refael, “Learning phase transitions from dynamics,” *Physical Review B* **98**, 060301 (2018).
 [17] Frank Schindler, Nicolas Regnault, and Titus Neupert, “Probing many-body localization with neural networks,” *Physical Review B* **95**, 245134 (2017).
 [18] Alireza Seif, Mohammad Hafezi, and Christopher Jarzynski, “Machine learning the thermodynamic arrow of time,” *Nature Physics* **17**, 105–113 (2021).
 [19] Jonathan Carifio, James Halverson, Dmitri Krioukov, and Brent D Nelson, “Machine learning in the string landscape,” *Journal of High Energy Physics* **2017**, 157 (2017).
 [20] Koji Hashimoto, Sotaro Sugishita, Akinori Tanaka, and Akio Tomiya, “Deep learning and the AdS/CFT correspondence,” *Phys. Rev. D* **98**, 046019 (2018).
 [21] Giuseppe Carleo and Matthias Troyer, “Solving the quantum many-body problem with artificial neural networks,” *Science* **355**, 602–606 (2017).
 [22] Giacomo Torlai, Guglielmo Mazzola, Juan Carrasquilla, Matthias Troyer, Roger Melko, and Giuseppe Carleo, “Neural-network quantum state tomography,” *Nature Physics* **14**, 447 (2018).
 [23] Juan Carrasquilla, Giacomo Torlai, Roger G Melko, and Leandro Aolita, “Reconstructing quantum states with generative models,” *Nature Machine Intelligence* **1**, 155 (2019).

- [24] Alireza Seif, Kevin A Landsman, Norbert M Linke, Caroline Figgatt, C Monroe, and Mohammad Hafezi, “Machine learning assisted readout of trapped-ion qubits,” *Journal of Physics B: Atomic, Molecular and Optical Physics* **51**, 174006 (2018).
- [25] Giacomo Torlai, Brian Timar, Evert PL van Nieuwenburg, Harry Levine, Ahmed Omran, Alexander Keesling, Hannes Bernien, Markus Greiner, Vladan Vuletić, Mikhail D Lukin, *et al.*, “Integrating neural networks with a quantum simulator for state reconstruction,” arXiv preprint arXiv:1904.08441 (2019).
- [26] Pasquale Calabrese and John Cardy, “Entanglement entropy and conformal field theory,” *Journal of Physics A: Mathematical and Theoretical* **42**, 504005 (2009).
- [27] Shu Tanaka, Ryo Tamura, and Hosho Katsura, “Entanglement spectra of the quantum hard-square model: Holographic minimal models,” *Phys. Rev. A* **86**, 032326 (2012).
- [28] Ian Goodfellow, Yoshua Bengio, and Aaron Courville, *Deep learning* (MIT press, 2016).
- [29] Diederik P Kingma and Jimmy Ba, “Adam: A method for stochastic optimization,” arXiv preprint arXiv:1412.6980 (2014).
- [30] Edward O’Brien and Paul Fendley, “Lattice supersymmetry and order-disorder coexistence in the tricritical ising model,” *Physical review letters* **120**, 206403 (2018).
- [31] Balázs Dóra, Rex Lundgren, Mark Selover, and Frank Pollmann, “Momentum-space entanglement and loschmidt echo in luttinger liquids after a quantum quench,” *Phys. Rev. Lett.* **117**, 010603 (2016).
- [32] Chia-Min Chung, Lars Bonnes, Pochung Chen, and Andreas M. Läuchli, “Entanglement spectroscopy using quantum monte carlo,” *Phys. Rev. B* **89**, 195147 (2014).
- [33] When H_e is far from criticality, our neural-network occasionally incorrectly predicts the sample data to be in one CFT class with very large probability. This is in sharp contrast to training with energy spectra. It would be interesting to see if this a fundamental problem with Rényi entropies or can be fixed by using more sophisticated techniques such as adversarial training.
- [34] JH Wilkinson, “The evaluation of the zeros of ill-conditioned polynomials. part ii,” *Numerische Mathematik* **1**, 167–180 (1959).
- [35] Ian Goodfellow, Yoshua Bengio, and Aaron Courville, *Deep Learning* (MIT Press, 2016) <http://www.deeplearningbook.org>.
- [36] Heng-Yu Chen, Yang-Hui He, Shailesh Lal, and M. Zaid Zaz, “Machine Learning Etudes in Conformal Field Theories,” arXiv e-prints, arXiv:2006.16114 (2020), arXiv:2006.16114 [hep-th].
- [37] T Mendes-Santos, X Turkeshi, M Dalmonte, and Alex Rodriguez, “Unsupervised learning universal critical behavior via the intrinsic dimension,” *Physical Review X* **11**, 011040 (2021).
- [38] Tiago Mendes-Santos, Adriano Angelone, Alex Rodriguez, Rosario Fazio, and Marcello Dalmonte, “Intrinsic dimension of path integrals: data mining quantum criticality and emergent simplicity,” arXiv preprint arXiv:2103.02640 (2021).
- [39] Joseph J. Bisognano and Eyvind H. Wichmann, “On the duality condition for a hermitian scalar field,” *Journal of Mathematical Physics* **16**, 985–1007 (1975), <https://doi.org/10.1063/1.522605>.
- [40] Peter D. Hislop and Roberto Longo, “Modular structure of the local algebras associated with the free massless scalar field theory,” *Communications in Mathematical Physics* **84**, 71–85 (1982).
- [41] Andreas M. Läuchli, “Operator content of real-space entanglement spectra at conformal critical points,” (2013), arXiv:1303.0741 [cond-mat.stat-mech].
- [42] Ananda Roy, Frank Pollmann, and Hubert Saleur, “Entanglement hamiltonian of the 1+1-dimensional free, compactified boson conformal field theory,” (2020), arXiv:2004.14370 [cond-mat.stat-mech].
- [43] John Cardy and Erik Tonni, “Entanglement hamiltonians in two-dimensional conformal field theory,” *Journal of Statistical Mechanics: Theory and Experiment* **2016**, 123103 (2016).
- [44] John L. Cardy, “Conformal invariance and surface critical behavior,” *Nuclear Physics B* **240**, 514–532 (1984).
- [45] John L. Cardy, “Effect of boundary conditions on the operator content of two-dimensional conformally invariant theories,” *Nuclear Physics B* **275**, 200 – 218 (1986).
- [46] Gil Young Cho, Ken Shiozaki, Shinsei Ryu, and Andreas W W Ludwig, “Relationship between symmetry protected topological phases and boundary conformal field theories via the entanglement spectrum,” *Journal of Physics A: Mathematical and Theoretical* **50**, 304002 (2017).
- [47] Davide Bianchini, O Castro-Alvaredo, Benjamin Doyon, Emanuele Levi, and Francesco Ravanini, “Entanglement entropy of non-unitary conformal field theory,” *Journal of Physics A: Mathematical and Theoretical* **48**, 04FT01 (2014).
- [48] Andrew Strominger, “The ds/cft correspondence,” *Journal of High Energy Physics* **2001**, 034 (2001).
- [49] Hugh Osborn and Andreas Stergiou, “C t for non-unitary cfts in higher dimensions,” *Journal of High Energy Physics* **2016**, 79 (2016).
- [50] Marcio Jose Martins, “A connection between integrable z (n) models and off-critical non-unitary theories,” *Physics Letters B* **240**, 404–406 (1990).
- [51] William Berdanier, Michael Kolodrubetz, Romain Vasseur, and Joel E Moore, “Floquet dynamics of boundary-driven systems at criticality,” *Physical review letters* **118**, 260602 (2017).
- [52] Xueda Wen and Jie-Qiang Wu, “Floquet conformal field theory,” arXiv preprint arXiv:1805.00031 (2018).
- [53] Xueda Wen and Jie-Qiang Wu, “Quantum dynamics in sine-square deformed conformal field theory: Quench from uniform to nonuniform conformal field theory,” *Physical Review B* **97**, 184309 (2018).
- [54] Rex Lundgren, Jonathan Blair, Pontus Laurell, Nicolas Regnault, Gregory A. Fiete, Martin Greiter, and Ronny Thomale, “Universal entanglement spectra in critical spin chains,” *Phys. Rev. B* **94**, 081112 (2016).
- [55] Michael Schuler, Seth Whitsitt, Louis-Paul Henry, Subir Sachdev, and Andreas M. Läuchli, “Universal Signatures of Quantum Critical Points from Finite-Size Torus Spectra: A Window into the Operator Content of Higher-Dimensional Conformal Field Theories,” *Phys. Rev. Lett.* **117**, 210401 (2016).
- [56] Seth Whitsitt and Subir Sachdev, “Transition from the Z_2 spin liquid to antiferromagnetic order: Spectrum on the torus,” *Phys. Rev. B* **94**, 085134 (2016).
- [57] Seth Whitsitt, Michael Schuler, Louis-Paul Henry, Andreas M. Läuchli, and Subir Sachdev, “Spectrum of the Wilson-Fisher conformal field theory on the torus,” *Phys. Rev. B* **96**, 035142 (2017).
- [58] Michael Schuler, Stephan Hesselmann, Seth Whitsitt, Thomas C. Lang, Stefan Wessel, and Andreas M. Läuchli, “Torus spectroscopy of the gross-neveu-yukawa quantum field theory: Free dirac versus chiral ising fixed point,” (2019), arXiv:1907.05373 [cond-mat.str-el].
- [59] Alex Thomson and Subir Sachdev, “Spectrum of conformal gauge theories on a torus,” *Phys. Rev. B* **95**, 205128 (2017).
- [60] Joshua D Qualls, “Lectures on conformal field theory,” arXiv preprint arXiv:1511.04074 (2015).

- [61] John L Cardy, “Operator content of two-dimensional conformally invariant theories,” *Nuclear Physics B* **270**, 186–204 (1986).
- [62] Michael Levin, “Protected edge modes without symmetry,” *Phys. Rev. X* **3**, 021009 (2013).
- [63] Charlotte Gils, Eddy Ardonne, Simon Trebst, David A Huse, Andreas WW Ludwig, Matthias Troyer, and Zhenghan Wang, “Anyonic quantum spin chains: Spin-1 generalizations and topological stability,” *Physical Review B* **87**, 235120 (2013).
- [64] Andrea Cappelli, Claude Itzykson, and JBJ Zuber, “The adic classification of minimal and $N=1$ conformal invariant theories,” *Communications in Mathematical Physics* **113**, 1–26 (1987).
- [65] Jacques Distler and Zongang Qiu, “Brs cohomology and a feigin-fuchs representation of $ka\check{c}$ -moody and parafermionic theories,” *Nuclear Physics B* **336**, 533–546 (1990).
- [66] Y Matsuo and S Yahikozawa, “Superconformal field theory with modular invariance on a torus,” *Physics Letters B* **178**, 211–218 (1986).
- [67] Elias B Kiritsis, “Character formulae and the structure of the representations of the $n=1$, $n=2$ superconformal algebras,” *International Journal of Modern Physics A* **3**, 1871–1906 (1988).